Electroabsorption by 0D, 1D, and 2D Nanocrystals: A Comparative Study of CdSe Colloidal Quantum Dots, Nanorods, and Nanoplatelets

Alexander W. Achtstein,[†] Anatol V. Prudnikau,[‡] Maxim V. Ermolenko,[§] Leonid I. Gurinovich,[§] Sergey V. Gaponenko,[§] Ulrike Woggon,[†] Alexander V. Baranov,[⊥] Mikhail Yu. Leonov,[⊥] Ivan D. Rukhlenko,[∥] Anatoly V. Fedorov,[⊥] and Mikhail V. Artemyev[‡,*]

[†]Institute of Optics and Atomic Physics, Technical University of Berlin, 10623 Berlin, Germany, [‡]Institute for Physico-Chemical Problems, Belarusian State University, 220030 Minsk, Belarus, [§]B. I. Stepanov Institute of Physics, National Academy of Sciences, 220072 Minsk, Belarus, [⊥]Saint Petersburg National Research University of Information Technologies, Mechanics and Optics, 197101 Saint Petersburg, Russia, and [∥]Monash University, Clayton, Victoria 3800, Australia

ABSTRACT This work presents a comprehensive study of electroabsorption in CdSe colloidal quantum dots, nanorods, and nanoplatelets. We experimentally demonstrate that the exposure of the nanoplatelets to a dc electric field leads to strong broadening of their lowest-energy heavy-hole absorption band and drastically reduces the absorption efficiency within the band. These are results of the quantum-confined Stark and Franz–Keldysh effects. The field-induced change in the nanoplatelets' absorption is found to be more than 10 times the change in the absorption by the quantum dots. We also demonstrate that the electroabsorption by the nanorods is weaker than that by the quantum dots and nanoplatelets and reveal an unusual dependence of the differential absorption changes on the nanoplatelet thickness: the thicker the nanoplatelet, the smaller the change.

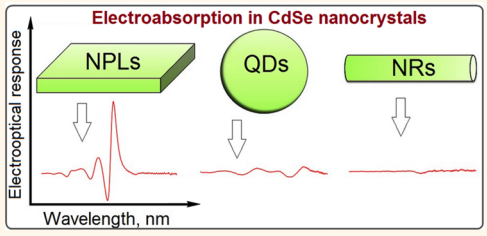

KEYWORDS: electroabsorption · quantum dots · nanorods · nanoplatelets · CdSe

The phenomenon of a change in the optical properties of semiconductor nanostructures in response to an electric field is employed in many photonics components—including electro-optic modulators[1−6] and switches[5,7] and self-electro-optic-effect devices.[8,9] The most widely employed electro-optic components are those based on the semiconductor quantum wells (QWs) that are fabricated using the chemical vapor deposition (CVD) or molecular beam epitaxy (MBE) technique.[2,10] When a static electric field is applied to a QW, it results in the quantum-confined Stark effect (QCSE)[11] and the quantum-confined Franz–Keldysh effect (QCFKE).[12] The former manifests itself in spectral shifts and broadening of the exciton absorption bands, as well as in changes in the intensities of the absorption maxima, whereas the latter leads to modulation of the absorption spectra and decrease of the interband transition energies. The field-induced changes in optical absorption and refractive index are the two main effects employed in electro-optic devices.

Over the past three decades, a pronounced QCSE has been observed in semiconductor quantum dots (QDs) and QWs that were grown in glass matrices, fabricated through MBE, or synthesized using the methods of colloidal chemistry.[13−24] The QCSE in the QD-based electro-optic absorbers operating in the near-infrared telecommunication range is still of high interest.[25−28] Electro-optic elements based on the semiconductor nanoparticles synthesized with colloidal chemistry have advantages over those prepared using the MBE or MBE-related techniques. First, the synthesis of such QDs is cheap, easy, and gives multigram quantities of QDs with controllable dimensions. Second, the spectral range of optical transitions can be tuned as required for a particular application

* Address correspondence to m_artemyev@yahoo.com.

Received for review December 14, 2013 and accepted August 8, 2014.

Published online August 08, 2014
10.1021/nn503745u

TABLE 1. Wavelengths of First Exciton Peaks and Geometric Parameters of CdSe Nanocrystals Used in the Electroabsorption Experiments

	nanoplatelets			quantum dots	nanorods	
first exciton peak (nm)	length (nm)	width (nm)	thickness (nm)	diameter (nm)	length (nm)	diameter (nm)
462	25	15	1.2 (4 MLs)			
464				2		
509				2.4		
512	20	15	1.5 (5 MLs)			
519					6	2.6
550				3	10	3.5
551	86	22	1.8 (6 MLs)			

via altering the size and chemical composition of the QDs. Besides these advantages, modern colloidal chemistry enables the creation of more or less exotic quantum nanostructures, such as semiconductor nanorods (NRs) or type II core−shell QDs with extended electron or hole energy states,[15,29−32] showing strong electro-optic response suitable for applications.

A new type of quantum nanocrystals—semiconductor nanoplatelets (NPLs)—has been recently synthesized using the methods of the high-temperature colloidal chemistry. NPLs are ultrathin and flat nanocrystals (typically made of CdSe, CdS, or CdTe) with lateral dimensions from a few to several tens of nanometers and thicknesses of several monolayers.[33−41] The strong anisotropic quantum confinement in the NPLs leads to extremely sharp peaks in the absorption and photoluminescence spectra of the NPLs at the room temperature. Since the lateral dimensions of NPLs are much larger than their thickness, the NPLs are the colloidal analogue of ultrathin semiconductor QWs prepared using the MBE.[42,43] This analogy suggests that colloidal NPLs could feature a strong electro-optic response desirable in optoelectronic applications.[1,2,7,8,44]

The ultrasmall thicknesses and nanometer-scale lateral dimensions of NPLs lead to a number of significant questions on (i) the structure of the NPLs' exciton and phonon energy spectra; (ii) the strengths of electron−phonon and electron−electron interactions inside them; and (iii) the modifications of the NPLs' exciton properties due to the surrounding dielectric matrix or external fields.[36,39,45] Since the MBE-fabricated QWs are well-known for their strong electro-optic effects,[1,2,7,8,44] it can be expected that colloidal NPLs would also demonstrate an enhanced electro-optical response.

This paper presents a comparative analysis of electroabsorption by the quantum-confined colloidal QDs, NRs, and NPLs made of CdSe. We reveal that the electro-optic response of the NPLs is about an order of magnitude stronger than that of QDs and NRs with the same energies of the optical transitions, and that the electroabsorption bands of the NPLs feature only minor spectral shifts but strong broadening. We also demonstrate that the NRs have the weakest electroabsorption as compared to QDs and NPLs and observe an unexpected strengthening of the NPLs' electro-optic response with the reduction in the NPLs' thickness.

RESULTS AND DISCUSSION

We synthesized three specimens of CdSe NPLs, two specimens of CdSe NRs, and three specimens of CdSe QDs using the standard route of the high-temperature colloidal chemistry (see Experimental Details). The thicknesses of the NPLs, the diameters and lengths of the NRs, and the diameters of the QDs were chosen so as to bring the energies of the first exciton transitions in all kinds of nanocrystals to three different spectral regions. The central wavelengths of the first exciton bands and geometric parameters of the nanocrystals in the specimens are summarized in Table 1. We were unable to synthesize the high-quality NRs with the first exciton band close to that (at 462 nm) of the thinnest NPLs, due to the extremely small NR diameters required.

Following the synthesis, all kinds of nanocrystals were embedded in thin polymeric films deposited on the surface of indium−tin−oxide (ITO)-coated glass. The second ITO electrode was attached to each polymeric film using epoxy glue, thus creating sandwich-like ITO/CdSe-NCs-in-polymer/epoxy/ITO structures. The volume concentration of CdSe in the polymer was less than 5%, and the distance between the ITO electrodes was about 40 μm in all samples. The exact values from a thickness measurement were used for determination of the applied field strength. The electro-optic response of the samples was measured using a commercial spectrophotometer and a high dc voltage power supply at the room temperature.

Figure 1a shows a representative set of linear absorption spectra $D(\lambda,F)$ for three NPL samples from Table 1 when the electric field applied to the samples is gradually increased from 0 to 125 kV/cm. Since these NPLs have lateral dimensions much larger than the lateral size of a heavy-hole exciton (about 5 nm), they exhibit only a weak lateral confinement.

The dominating features in the absorption spectra of Figure 1a are the lowest-energy heavy-hole (HH) and

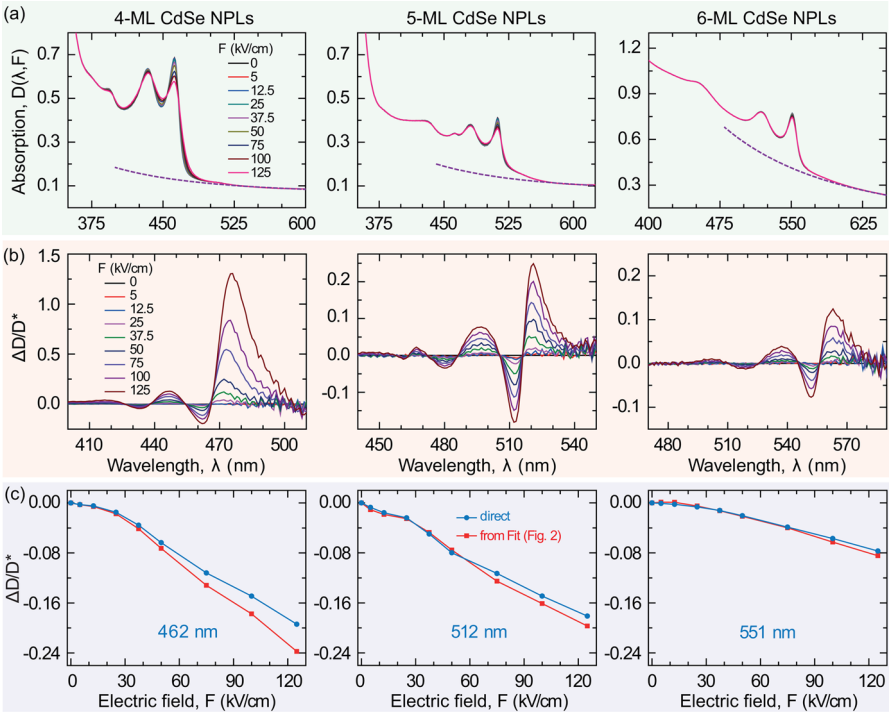

Figure 1. (a) Absorption spectra and (b) normalized differential absorption spectra of CdSe NPLs with 4, 5, and 6 monolayers (MLs) for different electric field strengths; first exciton peaks are located at 462, 512, and 551 nm, respectively (see Table 1). (c) Normalized differential absorption at wavelengths of 462, 512, and 551 nm deduced from (b) and from the fits in Figure 2a as functions of electric field strength. See text for details.

light-hole (LH) exciton transitions. The influence of an external electric field on these inhomogeneously broadened transitions is the subject of our study. The electric field strength F is defined as the ratio of the voltage applied to the ITO electrodes to the distance between the electrodes.

As Figure 1a suggests, the electric field substantially reduces the intensities of the first absorption peaks (at 460, 515, and 550 nm) and broadens the peaks without noticeably shifting them to longer wavelengths. The first two features are the classic footprints of the QCSE observed earlier in QWs and colloidal QDs.[2,19,21−24,46] However, the typical for QCSE red shift cannot be directly seen from the figure. This can be explained by the fact that the inhomogeneous broadening of the HH absorption band in the absence of a field is about 12 nm, which is much larger than the expected field-induced red shifts of the order of 1 meV (about 0.2 nm at the 512 nm wavelength). This article focuses on the field-induced changes of the amplitudes of the first excitonic absorption bands for which the spectral shifts much smaller than the full width at half-maximum (fwhm) values of the absorption bands are not relevant.

Since the electroabsorption spectra in Figure 1a are superimposed by a strong background due to the absorption by the polymer host and Rayleigh scattering at the NPLs and polymer inhomogeneities, a background correction is needed. The background contribution to the absorption spectrum of the n ML NPLs can be represented by the function $D_n(\lambda) = A_n/\lambda^4 + B_n$, in which the first term corresponds to Rayleigh scattering and the second to background absorption and sample reflectivity. The dashed curves in Figure 1a are the result of background fitting with $D_n(\lambda)$ at the low-energy side of the spectra. The fits give only rough estimates of the actual backgrounds at the high-energy sides of the absorption spectra but are quite accurate for wavelengths in the vicinity of the two lowest-energy exciton peaks corresponding to the transitions from the subbands of heavy and light holes. We therefore characterize the efficiency of electroabsorption near these peaks through the background-corrected, normalized differential absorption spectrum defined as

$$\frac{\Delta D}{D^*} = \frac{D(\lambda, F) - D(\lambda, 0)}{D(\lambda, 0) - D_n(\lambda)} \quad (1)$$

The normalized differential absorption spectra of the NPLs are shown in Figure 1b for different field strengths. The field-induced changes in the oscillator strengths of the exciton transitions—characterized by the minima of $\Delta D/D^*$—are seen to decrease with the NPL thickness. The normalized electroabsorption signal at 462, 512, and 551 nm, corresponding to the first excitonic transition in the three NPL samples, is plotted as a function of the electric field strength in Figure 1c. It is seen that the increase of the NPL thickness from 4 to 6 monolayers (MLs) results in about a 2.5-fold decrease of $|\Delta D/D^*|$. This behavior of the electroabsorption signal disagrees with the predictions of simple theoretical models of the QCSE in QWs[11] according to which a

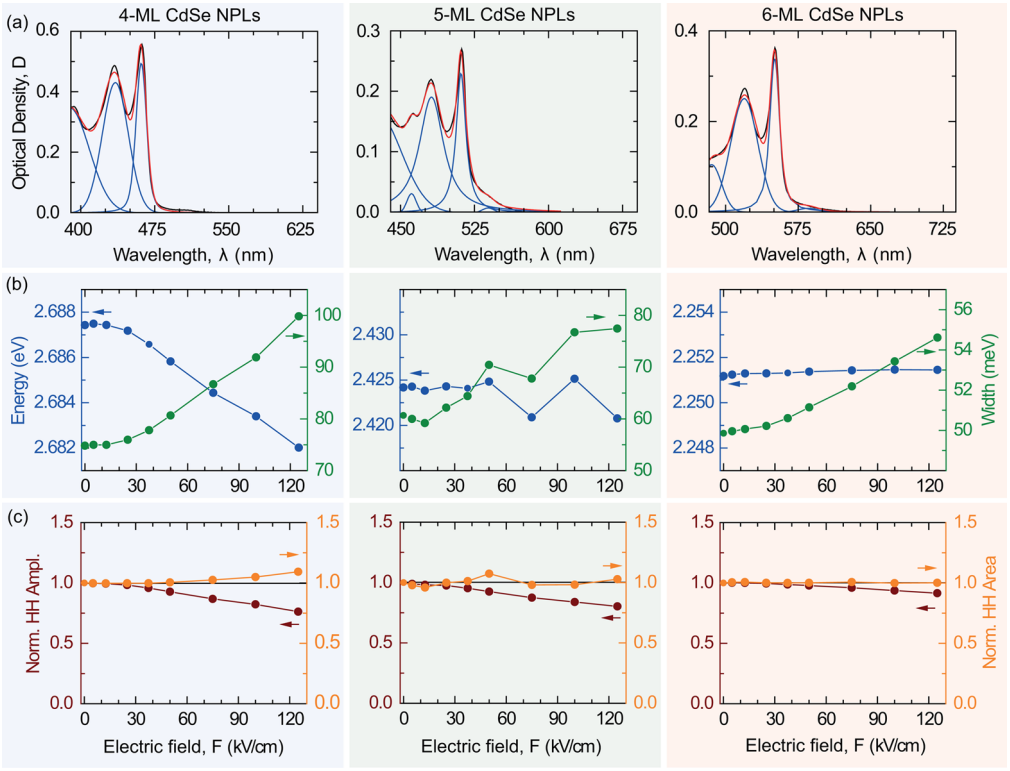

Figure 2. (a) Absorption spectra of 4, 5, and 6 ML CdSe NPLs in the absence of an electric field (black curves) corrected with $D_n(\lambda)$ from Figure 1, and multicomponent fits to the HH, LH, and split-off bands. (b) Absorption energy and line width of the first HH exciton transition from the fits in (a). (c) Normalized amplitude and area under the first HH exciton peak from the fits in (a). The black lines in (c) correspond to zero field.

small increase in the NPL thickness should lead to a slight increase in $|\Delta D/D^*|$.

Since the differential absorption spectra in Figure 1a, b show indications of a field-dependent change of the absorption band amplitudes and a field-induced broadening, we analyze in Figure 2 the field dependence of the absorption spectra after background and scattering corrections with $D_n(\lambda)$ (taken from Figure 1a). To fit the corresponding HH, LH, and split-off band contributions, we model the first HH exciton transition by a Voigt profile and the other transitions by Gaussians (all shown in blue). In the 5 ML case, we include a fourth peak around 462 nm to take into account a small fraction of 4 ML NPL in the 5 ML NPL sample. A Gaussian defect band below the first exciton HH transition is also included to allow for the lower-energy defect emission.

Figure 2a shows the absorption spectra at zero voltage (black curves), the component fits (blue curves), and the fit spectra (red curves). Figure 2b shows the results of these fits for the first HH transition energy and the inhomogeneous transition line width at varying external field strengths. In Figure 2c, the amplitudes of the fitted HH transition as well as their integrated areas normalized to the zero field case are displayed.

Figure 2b shows that the HH absorption peak of the 4 ML NPL exhibits a distinct field-induced red shift. This is consistent with the QCSE-based predictions of Miller *et al.*[11,47] for QWs. The red shifts measured for the 5 ML and 6 ML NPLs are less pronounced than those of the 4 ML NPL and CdSe NRs, which can be fitted by the sum $\Delta E = \mu F + \alpha F^2$, where F is the electric field strength and μ and α are the dipole moment and polarizability of the excited state, respectively.[16] Note that the absolute value of the field-induced spectral shifts cannot be determined exactly since the observed shifts are in the range of the 2 meV resolution of the absorption spectrometer. This may also be the reason for observation of only a tendential decrease of the exciton energy with applied field in the 5 ML NPL samples.

For a given spectral resolution, a significant broadening of the HH exciton emission can be observed for all NPL thicknesses. Figure 2b shows that the widths of the HH absorption bands increase with the applied electric field by factors ranging from 1.1 to 1.34. As a general trend, we observe a reduction of the field-induced broadening with the NPL thickness. It is not possible to deduce directly from the experiment whether the broadening is due to the field inhomogeneity within the randomly oriented NPL ensemble, dispersion of the NPL lateral sizes, or a more basic physical reason related to the modification of the exciton wave function by an external field. Miller *et al.*[47] pointed out that it is generally difficult to distinguish between the impacts of inhomogeneity effects and direct broadening effects on the exciton wave function.

The observed line broadening raises the question whether the strong electroabsorption changes occur due to this broadening or the field-induced change in the HH transition oscillator strength. This question is answered by Figure 2c, where we plot the field dependencies of the normalized amplitude of the fitted HH transition component and the corresponding normalized area of the component (both deduced from Figure 2a).

As we have seen from the $\Delta D/D$ spectra in Figure 1, the amplitudes of the HH absorption peaks decrease with the external field strength and NPL thickness. Since the spectral widths of the HH absorption peaks grow with the field, these amplitudes cannot be used as a measure of the field-induced changes. We therefore also plot the normalized (to zero field from the fits in Figure 2a) integrated area of the HH absorption band *versus* the applied field in Figure 2c. The changes of this area characterize the relative changes in the spectrally integrated HH oscillator strength. The oscillator strength change at 125 kV/cm is seen to be less than 10% for 4 ML NPLs and very low for thicker (5 ML and 6 ML) NPLs. In all cases, the field-induced amplitude changes (of 26% for 4 ML NPLs, 20% for 5 ML NPLs, and 8% for 6 ML NPLs) are much larger than the respective relative changes of the integrated oscillator strength. This leads to a conclusion that the observed strong electro-optic modulation is mainly a result of the field-induced broadening, whereas the field-induced changes of the transition oscillator strength play only a minor role. One can also see that the broadening and amplitude change decrease with the NPL thickness, in line with Figure 1c.

The unusual trend of a reduction of the electro-optic response exhibited by the size dependency of the NPLs can be accounted for by supposing that the dielectric screening of the in-plane external fields is negligible in ultrathin NPLs and grows with their thickness. In this case, the electro-optic effect weakens with the NPL thickness and the observed thickness dependency is qualitatively similar to the expected one. As the NPLs become thicker, the dielectric screening increases due to a decreasing local Lorentz field factor and the local field in the NPLs becomes smaller. This can explain the weakening of the electro-optic effect in thicker NPLs.

It is also seen from Figure 1c that the results of the $\Delta D/D$ determination from the direct differential absorption spectra (Figure 1b) and the fitting method (Figure 2) are in good agreement. Minor differences occur since a small contribution of the LH exciton to the absorption at the HH energy cannot be taken into account with the first method.

As already stated, Figure 1c shows that, with both evaluation methods, the corresponding $\Delta D/D$ signal of the NPLs does not follow precisely a quadratic field dependency, as it occurs in the case of the classical QCSE in weak electric fields.[19] This indicates that the physics behind the QCSE in two-dimensional colloidal nanocrystals is more complex than in QDs or bulk semiconductors.

To this point, we have not discussed the nature of the photoexcited states in the NPLs. Since the exciton binding energies in these two-dimensional QWs are on the order of 150 meV, as Achtstein *et al.*[36] have shown in calculations, these are mostly excitons that are present in the NPLs, whereas free electron−hole pairs form a negligible fraction. Kunneman *et al.*[48] showed that, even at room temperature, excitons are the dominating species in CdSe NPLs, which is also suggested by the existence of sharp excitonic peaks in the absorption spectra (in contrast, electron−hole pair dominated NPLs would have step-like absorption spectra). So the observed field-induced changes of the HH and LH exciton transition bandwidth and dipole moments are due to the polarization of the exciton, resulting in the field-induced broadening and a minor decrease of the transition overlap integral.

Due to the highly anisotropic electronic confinement in the NPLs and their random orientation in the samples, two effects are present at the same time: the lateral QCFKE for the in-plane field components and the QCSE for the transversal field components. Since the lateral extent of the NPLs is much larger than the exciton Bohr radius,[36] the excitons experience almost no confinement in the lateral direction so that the QCFKE dominates the in-plane fields. The QCSE is observed for perpendicular field orientations due to the strong spatial confinement of the exciton wave function in this direction. The spectral shifts due to the QCSE and QCFKE are expected to be low, in line with our experimental results. This is also consistent with the results of Pedersen and Lynge,[49] who showed that the spectral shift of the first exciton transition in an external field nearly vanishes in an inhomogeneously broadened ensemble of NRs.

The reduction of the electro-optic response for thicker NPLs observed in our experiments is not a result of a variation of the exciton binding energy, which is relevant for exciton ionization, because this energy is expected to decrease with layer thickness.[36] An increased electro-optic response would occur in this case in contrast to the observations.

The increasing thickness of the NPLs results further in reduction of the internal electric fields due to a stronger dielectric screening since the local field factor for parallel orientation decreases with the NPL thickness. Therefore, thin NPLs exhibit the strongest electro-optic response. For other nanoparticle shapes, like NRs and QDs, the lower angularly averaged local field factors[50] result in weaker internal electric fields in the nanoparticles and, thus, in a decreased electro-optic effect. In Figure 3, we study under the same conditions a set of CdSe QDs and NRs with first exciton transition energies close to the energies of the first exciton peaks of the NPLs. The transmission electron microscopy (TEM) images of the NRs and NPLs used in this study are shown in Figure 3c−g.

Figure 3a,b shows the measured linear and normalized differential absorption spectra for F = 125 kV/cm.

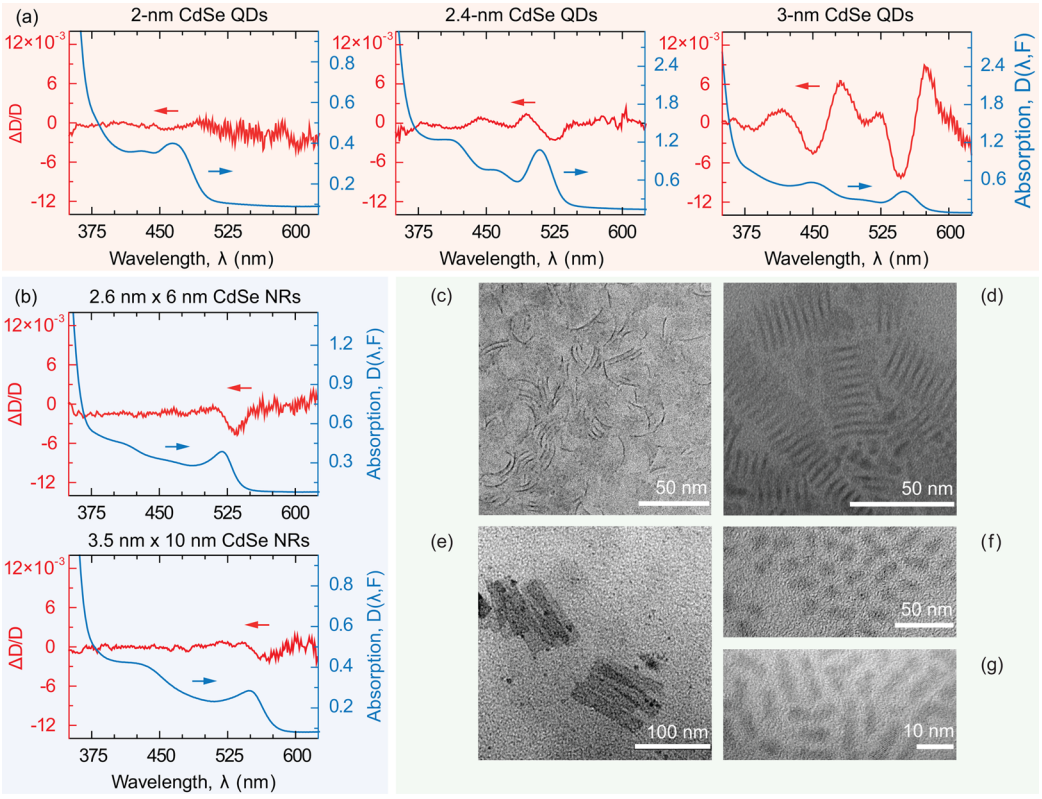

Figure 3. Linear (blue) and normalized (red) differential absorption spectra of CdSe (a) QDs and (b) NRs for $F = 125$ kV/cm, and TEM images of (c) 4 ML NPLs, (d) 5 ML NPLs, (e) 6 ML NPLs, (f) 2.6 nm × 6 nm NRs, and (g) 3.5 nm × 10 nm NRs (see Table 1).

The spectra are corrected for background and scattering only in case of the NPLs since the background offsets for QDs and NRs are relatively small. We obtain a significantly lower electro-optic responses in these samples as compared to those of the NPLs. It can also be seen that $\Delta D/D$ grows with the QD size. This trend is opposite to that for the NPLs but in line with the size dependency reported by Stokes *et al.*[51] and Colvin *et al.*[19] Surprisingly, the electroabsorption efficiency in the NRs is even several times less than that in the QDs. This result is in agreement with previously published data,[31] where QDs and NRs of larger sizes were compared. These published data additionally support that QDs exhibit a higher electroabsorption response than NRs and that large QDs have higher sensitivity to external fields than the smaller ones.

Figure 3 also shows that, with increasing confinement of the QD exciton wave function, the electro-optic effect becomes less pronounced. So the strong spatial confinement in QDs and NRs hinders the spatial separation of the electron and hole wave functions under the applied field, resulting in reduced broadening and smaller decrease of the transition dipole moment. The lower broadening and oscillator strength change of the HH absorption band lead to a smaller electro-optic response of QDs and NRs. Since the lateral extent of the NPLs is much larger than the diameter/length of the NRs and QDs, the electron and hole wave functions can be much more distorted in the NPLs, resulting in a much stronger electro-optic response with pronounced broadening.

Generally, the relative change in the field-induced absorption is mainly governed by the longest extend of the particles along the *x*, *y*, or *z* axis. Therefore, the long NPLs show considerably higher electroabsorption changes as compared to the more compact QDs of comparable emission wavelengths. In the case of the NPLs, the spatial separation of the electron and hole wave function in the applied field can be much larger, resulting in larger broadening and transition oscillator strength change.

Figure 4 shows the differential absorption at the first exciton peak for all nanocrystals from Table 1 (in the case of the NPLs, the $\Delta D/D$ values from the fits in Figure 2a are used). The field-induced relative change in the absorption by the NPLs is seen to be on the order of 0.1, which is much larger than the change (less than 0.01) for QDs and NRs.

The comparison of the normalized differential absorption by QDs and NPLs shows that the strength of their electro-optic response is mainly determined by the largest nanocrystal extent. Therefore, NPLs exhibit the strongest electroabsorption and are most promising for electro-optic applications like modulators. The CdSe NPL-based materials can be used in Mach–Zender interferometer-based modulators, which do not use the direct changes in absorption but employ the Kramers–Kronig relations between refractive index and phase changes (even apart from the excitonic resonance).

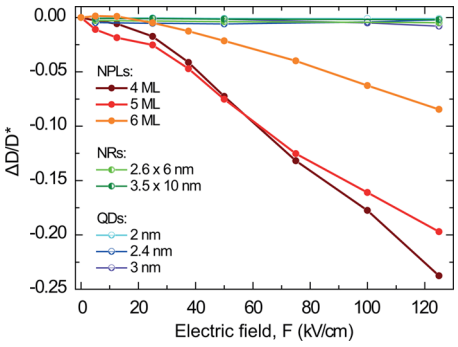

Figure 4. Normalized differential absorption by CdSe NPLs, QDs, and NRs from Table 1. The NPL results are taken from Figure 1c for the case $\Delta D/D^*$ determination by fitting (from Figure 2a). The results for NRs and QDs are taken directly from the differential absorption spectra given in Figure 3 and for the corresponding field values.

The experimental findings for NPLs, NRs, and QDs are complex and require a treatment by an elaborate theory of electroabsorption in these low-dimensional structures, which should take into account different responses of the electronic systems of the structures to an external electric field. The coexistence of excitons and free electron–hole pairs in the NPLs is also an important factor to be allowed for by the theory. As indicated by the results of Kunneman *et al.*,[48] excitons are the dominating quasiparticles in CdSe NPLs even at room temperature. Since the binding energy of a quasi-two-dimensional exciton decreases with the NPL thickness, so does the ratio of excitons to free electron–hole pairs. Therefore, a (changing) fraction of strongly polarizable electron–hole pairs may contribute to the extreme NPL sensitivity to the electric field and the observed thickness dependency. It is expected that the density of free carriers generated through electroabsorption in the NPL samples is low, and that the electro-optic effect is predominantly caused by the polarization of excitons. However, the much lower exciton binding energies in the QD and NR samples make an absorption contribution by the generation of electron–hole pairs more probable.

The strongly enhanced electroabsorption of NPLs as compared to QDs and NRs is also a result of the dielectric screening by different particle shapes. In the limiting cases of infinitely thin and long NPLs or NRs, the in-plane or parallel orientation Lorentz local field factor approaches unity, so that the dielectric screening of the external field vanishes in these directions. Since the probability for a randomly oriented NPL to be parallel to the external field is higher than that for a NR to be oriented parallel to its long axis, the field screening is stronger in NRs compared to NPLs. Besides the impact on the electronic system, this results in a higher electro-optic response of NPLs as compared to NRs and QDs.

CONCLUSIONS

We have studied the electroabsorption by CdSe NPLs, NRs, and QDs and observed that the NPLs exhibit a much stronger electro-optical response than do the NRs and QDs. The reason behind the strong response is that the efficiency of electroabsorption is governed by the largest nanocrystal dimension, resulting in a maximal electro-optic response for the NPLs. We also demonstrated that the NRs exhibit the weakest electroabsorption as compared to the NPLs and QDs, which may be explained by the strong dielectric screening of the external electric field in a randomly oriented nanoparticle ensemble and the strong spatial confinement of the electron and hole wave functions. We also observed that the electro-optic response of the NPLs weakens with their thickness. This may be a result of a decrease in the internal electric field due to a lower local field factor with increasing thickness.

The observed strong electroabsorption by the CdSe NPLs makes them a promising material for electro-optic devices analogous to those based on semiconductor QWs prepared using the MBE. Unlike the MBE-grown QWs, colloidal NPLs may be prepared in large quantities and embedded in thin polymer films of large surface areas. Moreover, in addition to the much stronger electro-optic response of the NPLs as compared to the other kinds of colloidal nanocrystals, they possess sharp exciton absorption bands, which significantly benefits the performance of refractive electro-optic modulators. The realization of the full potential associated with the pronounced electro-optic effect in the NPLs would require the development of advanced techniques for the synthesis of colloidal NPLs absorbing in the near-infrared telecommunication region.

A detailed modeling of the electric field impact on NPLs, including the excitonic and local field effects, requires a great deal of research efforts and deserves a separate publication. In particular, an advanced theoretical model of electroabsorption has to allow for the coexistence of excitons and electron–hole pairs in NPLs, external field screening, and surface polarization effects, which are absent in most epitaxial structures. This would lead to a precise description of the effects observed in our experiments. Such a detailed modeling is beyond the scope of this paper and will be reported elsewhere.

METHODS

Experimental Details. *Materials.* Cadmium oxide powder (99.5%), cadmium acetate, zinc acetate dehydrate, 2-ethylhexanoic acid, stearic acid (95%), 1-octadecene (90%), trioctylphosphine (97%), trioctylphosphine oxide (90%), poly(maleic anhydride-*alt*-1-octadecene) of average M_n between 30 000 and 50 000, selenium powder, and ITO-coated glass slides of 70–100 Ω/sq resistivity were purchased from Sigma-Aldrich; *n*-hexadecylphosphonic

acid was purchased from Plasmachem (www.plasmachem.com).

CdSe NPLs with the first exciton absorption bands at 462, 512, and 551 nm were synthesized similarly to how it was done by Cherevkov *et al.*[45]

4 ML CdSe NPLs with the First Exciton Transition at 462 nm. 0.4 mmol of cadmium acetate, 0.1 mmol of stearic acid, 0.1 mg of selenium powder, and 10 mL of 1-octadecene were loaded in a three-neck reaction flask, degassed for 30 min at room temperature, and heated to 180 °C in an argon atmosphere. The reaction was stopped after 20 min by cooling the mixture to 80 °C, and the NPLs were deposited with isopropyl alcohol.

5 ML CdSe NPLs with the First Exciton Transition at 512 nm. 0.3 mmol of cadmium oxide, 0.72 mmol of myristic acid, and 2 mL of 1-octadecene were loaded in a three-neck reaction flask and heated to a complete dissolution of the oxide. This was followed by the addition of 13 mL of 1-octadecene and degassing of the reaction mixture for 30 min at 120 °C. The flask was then purged with argon, cooled to the room temperature, and 0.12 mmol of selenium powder was added to the mixture. The mixture was heated rapidly, and 0.25 mmol of zinc acetate dehydrate was added to it when its temperature reached 190 °C. The mixture was then heated further to 240 °C and kept at this temperature for 5 min. The reaction was stopped by cooling the flask to 80 °C, and the NPLs were deposited with isopropyl alcohol.

6 ML CdSe NPLs with the First Exciton Transition at 551 nm. 0.3 mmol of cadmium oxide, 0.72 mmol of myristic acid, and 2 mL of 1-octadecene were loaded in a three-neck reaction flask and heated to a complete dissolution of the oxide. This was followed by the addition of 13 mL of 1-octadecene and degassing of the reaction mixture for 30 min at 120 °C. The flask was then purged with argon, heated to 240 °C, and 0.15 mmol of selenium suspension in 1 mL of 1-octadecene was added to the mixture. After 40 s, 0.5 mmol of cadmium acetate was added to the mixture, which was was kept for 12 min at 240 °C afterward. The reaction was stopped by cooling the mixture to 80 °C, and the NPLs were deposited with isopropyl alcohol.

CdSe QDs with the First Exciton Transition at 464 nm. 0.5 mmol of cadmium oxide, 1 mL of 2-ethylhexanoic acid, and 2 mL of 1-octadecene were loaded into a three-neck flask and heated to a complete dissolution of the oxide. Then, 110 mg of *n*-hexadecylphosphonic acid and 7 mL of 1-octadecene were added, and the reaction mixture was degassed at 100 °C in an argon atmosphere. The mixture was then heated further to 290 °C, and 0.5 mmol of Se (dissolved in the mixture of 0.7 mmol of trioctylphosphine and 1 mL of 1-octadecene) was injected into the mixture under intense stirring. The flask was then rapidly cooled to 200 °C under vigorous stirring in the argon atmosphere and left for 4 min to enable the formation of the QDs.

CdSe QDs with the First Exciton Transitions at 509 and 550 nm were synthesized similar to how it was done by Sun *et al.*[52] The size of the QDs was controlled by the concentration of the aliphatic acids and the reaction temperature.

CdSe NRs with the First Exciton Transitions at 519 and 550 nm were synthesized similar to how it was done by Prudnikau *et al.*[53] The size of the NRs was controlled by the concentration of the hexadecylphosphonic acid and the reaction temperature.

The as-synthesized CdSe NPLs, QDs, and NRs were additionally purified *via* the methanol-assisted deposition from their solutions in chloroform and then dissolved in pure chloroform by the addition of polymer [5 mg of poly(maleic anhydride-*alt*-1-octadecene) in 1 mL of chloroform]. The resulting solutions were centrifuged at 1000 rpm for several minutes to remove possible aggregates and drop-casted onto the ITO/glass substrate. The polymer films were quickly dried under vacuum, and the second ITO/glass electrodes were attached to them using transparent epoxy glue. The thicknesses of the polymeric films containing the nanocrystals were about 20 μm. The total distance between the two electrodes was about 40 μm in all samples. All thicknesses were determined with 1 μm accuracy using a micrometer.

A dc electric field was generated between the ITO electrodes using the stabilized voltage source HVPS-320 (Spetspribor). The optical absorption spectra were recorded in the 350−650 nm spectral range at room temperature using a Cary 500 (Varian) spectrophotometer.

Conflict of Interest: The authors declare no competing financial interest.

Acknowledgment. A.A. and U.W. acknowledge the financial support from DFG project Wo477/32-1. L.I., S.G., and M.A. acknowledge the financial support from the "Electronics and Photonics" program. A.P. acknowledges BRFFI Grant X13M-017. A.V.B., M.Yu.L., I.D.R., and A.V.F. gratefully acknowledge the financial support from the Ministry of Education and Science of the Russian Federation, Grant 14.B25.31.0002. The work of I.D.R. is sponsored by the Australian Research Council, through its Discovery Early Career Researcher Award DE120100055.

REFERENCES AND NOTES

1. Thoma, J.; Liang, B.; Reyner, C.; Ochalski, T.; Williams, D.; Hegarty, S. P.; Huffaker, D.; Huyet, G. Electro-optic Properties of GaInAsSb/GaAs Quantum Well for High-Speed Integrated Optoelectronic Devices. *Appl. Phys. Lett.* **2013**, *102*, 013120.
2. Cunningham, J. E. Recent Developments and Applications in Electroabsorption Semiconductor Modulators. *Mater. Sci. Eng.* **1999**, *25*, 155–194.
3. Babucke, H. ZnSe-Based Electro-optic Waveguide Modulators for the Blue-Green Spectral Range. *Semicond. Sci. Technol.* **1998**, *13*, 200–206.
4. Michler, P. Quantum Confined Stark Effect of II−VI Heterostructures Suitable as Modulators in the Blue-Green Spectral Region. *Appl. Phys. Lett.* **1998**, *72*, 3320–3322.
5. Miller, D. A. B. In *Confined Electrons and Photons*; Burstein, B., Weisbuch, C., Eds.; Plenum Press: New York, 1995; pp 675−701.
6. Kawakami, Y. II−VI Quantum-Confined Stark Effect Modulator. *Physica B* **1993**, *185*, 496–499.
7. Ikehara, H.; Goto, T.; Kamiya, H.; Arakawa, T.; Kokubun, Y. Hitless Wavelength-Selective Switch Based on Quantum Well Second-Order Series-Coupled Microring Resonators. *Opt. Express* **2013**, *21*, 6377–6390.
8. Tasso, I. V. M.; De Souza, E. A. Towards Local Motion Detection by the Use of Analog Self Electro-optic Effect Device. *Opt. Express* **2010**, *18*, 8000–8005.
9. Miller, D. A. B. Quantum-Well Self-Electro-optic Effect Devices. *Opt. Quantum Electron.* **1990**, *22*, S61–S98.
10. Partovi, A.; Glass, A. M.; Olson, D. H.; Feldman, R. D.; Austin, R. F.; Lee, D.; Johnson, A. M.; Miller, D. A. B. Electroabsorption in II−VI Multiple Quantum Wells. *Appl. Phys. Lett.* **1991**, *58*, 334–336.
11. Miller, D. A. B.; Chemla, D. S.; Damen, T. C.; Gossard, A. C.; Wiegmann, W.; Wood, T. H.; Burrus, C. A. Band-Edge Electroabsorption in Quantum Well Structures: The Quantum-Confined Stark Effect. *Phys. Rev. Lett.* **1984**, *53*, 2173–2176.
12. Miller, D. A. B.; Chemla, D. S.; Schmitt-Rink, S. Relation between Electroabsorption in Bulk Semiconductors and in Quantum Wells: The Quantum-Confined Franz−Keldysh Effect. *Phys. Rev. B* **1986**, *33*, 6976–6982.
13. Achtstein, A. W.; Karl, H.; Stritzker, B. Field Induced Photoluminescence Quenching and Enhancement of CdSe Nanocrystals Embedded in SiO_2. *Appl. Phys. Lett.* **2006**, *89*, 061103.
14. Achtstein, A.; Karl, H.; Stritzker, B. Electric-Field-Controlled Photoluminescence of CdSe Nanocrystal-Doped SiO_2 on Si. *J. Lumin.* **2006**, *121*, 365–368.
15. Artemyev, M. V.; Woggon, U.; Jaschinski, H.; Gurinovich, L. I.; Gaponenko, S. V. Spectroscopic Study of Electronic States in an Ensemble of Close-Packed CdSe Nanocrystals. *J. Phys. Chem. B* **2000**, *104*, 11617–11621.
16. Empedocles, S. A.; Bawendi, M. G. Quantum-Confined Stark Effect in Single CdSe Nanocrystallite Quantum Dots. *Science* **1997**, *278*, 2114–2117.
17. Artemyev, M. V.; Yablonski, G. P.; Rakovich, Y. P. Luminescence Spectra of Quantum-Sized CdS and PbI_2 Particles in Static Electric-Field. *Acta Phys. Polym., A* **1995**, *87*, 523–527.

18. Dissanayake, A. S.; Lin, J. Y.; Jiang, H. X. Quantum-Confined Stark Effects in $CdS_{1-x}Se_x$ Quantum Dots. *Phys. Rev. B* **1995**, *51*, 5457–5460.
19. Colvin, V. L.; Cunningham, K. L.; Alivisatos, A. P. Electric-Field Modulation Studies of Optical-Absorption in CdSe Nanocrystals—Dipolar Character of the Excited-State. *J. Chem. Phys.* **1994**, *101*, 7122–7138.
20. Woggon, U.; Bogdanov, S. V.; Wind, O.; Schlaad, K. H.; Pier, H.; Klingshirn, C.; Chatziagorastou, P.; Fritz, H. P. Electro-optic Properties of CdS Embedded in a Polymer. *Phys. Rev. B* **1993**, *48*, 11979–11986.
21. Colvin, V. L.; Alivisatos, A. P. CdSe Nanocrystals with a Dipole-Moment in the First Excited-State. *J. Chem. Phys.* **1992**, *97*, 730–733.
22. Cotter, D.; Burt, M. G.; Girdlestone, H. P. Electroabsorptive Behavior of Semiconductor Quantum Dots in Glass. *Semicond. Sci. Technol.* **1990**, *5*, 631–633.
23. Ekimov, A. I.; Efros, A. L.; Shubina, T. V.; Skvortsov, A. P. Quantum-Size Stark-Effect in Semiconductor Microcrystals. *J. Lumin.* **1990**, *46*, 97–100.
24. Hache, F.; Ricard, D.; Flytzanis, C. Quantum-Confined Stark-Effect in Very Small Semiconductor Crystallites. *Appl. Phys. Lett.* **1989**, *55*, 1504–1506.
25. Liu, X.; Iimori, T.; Ohshima, R.; Nakabayashi, T.; Ohta, N. Electroabsorption Spectra of PbSe Nanocrystal Quantum Dots. *Appl. Phys. Lett.* **2011**, *98*, 161911.
26. Piwonski, T.; Pulka, J.; Viktorov, E. A.; Huyet, G.; Houlihan, J. Refractive Index Dynamics of Quantum Dot Based Waveguide Electroabsorbers. *Appl. Phys. Lett.* **2010**, *97*, 051107.
27. Lumb, M. P.; Clarke, E.; Harbord, E.; Spencer, P.; Murray, R.; Masia, F.; Borri, P.; Langbein, W.; Leburn, C. G.; Jappy, C.; *et al.* Ultrafast Absorption Recovery Dynamics of 1300 nm Quantum Dot Saturable Absorber Mirrors. *Appl. Phys. Lett.* **2009**, *95*, 041101.
28. Klem, E. J. D.; Levina, L.; Sargent, E. H. PbS Quantum Dot Electroabsorption Modulation across the Extended Communications Band 1200−1700 nm. *Appl. Phys. Lett.* **2005**, *87*, 053101.
29. Yaacobi-Gross, N.; Garphunkin, N.; Solomeshch, O.; Vaneski, A.; Susha, A. S.; Rogach, A. L.; Tessler, N. Combining Ligand-Induced Quantum-Confined Stark Effect with Type II Heterojunction Bilayer Structure in CdTe and CdSe Nanocrystal-Based Solar Cells. *ACS Nano* **2012**, *6*, 3128–3133.
30. Park, K.; Deutsch, Z.; Li, J. J.; Oron, D.; Weiss, S. Single Molecule Quantum-Confined Stark Effect Measurements of Semiconductor Nanoparticles at Room Temperature. *ACS Nano* **2012**, *6*, 10013–10023.
31. Gurinovich, L. I.; Lutich, A. A.; Stupak, A. P.; Prislopsky, S. Y.; Rusakov, E. K.; Artemyev, M. V.; Gaponenko, S. V.; Demir, H. V. Luminescence in Quantum-Confined Cadmium Selenide Nanocrystals and Nanorods in External Electric Fields. *Semiconductors* **2009**, *43*, 1008–1016.
32. Becker, K.; Lupton, J. M.; Mueller, J.; Rogach, A. L.; Talapin, D. V.; Weller, H.; Feldmann, J. Electrical Control of Forster Energy Transfer. *Nat. Mater.* **2006**, *5*, 777–781.
33. Griffin, G. B.; Ithurria, S.; Dolzhnikov, D. S.; Linkin, A.; Talapin, D. V.; Engel, G. S. Two-Dimensional Electronic Spectroscopy of CdSe Nanoparticles at Very Low Pulse Power. *J. Chem. Phys.* **2013**, *138*, 014705.
34. Bouet, C.; Tessier, M. D.; Ithurria, S.; Mahler, B.; Nadal, B.; Dubertret, B. Flat Colloidal Semiconductor Nanoplatelets. *Chem. Matter.* **2013**, *25*, 1262–1271.
35. Mahler, B.; Nadal, B.; Bouet, C.; Patriarche, G.; Dubertret, B. Core/Shell Colloidal Semiconductor Nanoplatelets. *J. Am. Chem. Soc.* **2012**, *134*, 18591–18598.
36. Achtstein, A. W.; Schliwa, A.; Prudnikau, A.; Hardzei, M.; Artemyev, M. V.; Thomsen, C.; Woggon, U. Electronic Structure and Exciton−Phonon Interaction in Two-Dimensional Colloidal CdSe Nanosheets. *Nano Lett.* **2012**, *12*, 3151–3157.
37. Pelton, M.; Ithurria, S.; Schaller, R. D.; Dolzhnikov, D. S.; Talapin, D. V. Carrier Cooling in Colloidal Quantum Wells. *Nano Lett.* **2012**, *12*, 6158–6163.
38. Ithurria, S.; Bousquet, G.; Dubertret, B. Continuous Transition from 3D to 1D Confinement Observed during the Formation of CdSe Nanoplatelets. *J. Am. Chem. Soc.* **2011**, *133*, 3070–3077.
39. Ithurria, S.; Tessier, M. D.; Mahler, B.; Lobo, R. P. S. M.; Dubertret, B.; Efros, A. L. Colloidal Nanoplatelets with Two-Dimensional Electronic Structure. *Nat. Mater.* **2011**, *10*, 936–941.
40. Li, Z.; Peng, X. Size/Shape-Controlled Synthesis of Colloidal CdSe Quantum Disks: Ligand and Temperature Effects. *J. Am. Chem. Soc.* **2011**, *133*, 6578–6586.
41. Ithurria, S.; Dubertret, B. Quasi 2D Colloidal CdSe Platelets with Thicknesses Controlled at the Atomic Level. *J. Am. Chem. Soc.* **2008**, *130*, 16504–16505.
42. Yoshikawa, A.; Che, S. B.; Yamaguchi, W.; Saito, H.; Wang, X. Q.; Ishitani, Y.; Hwang, E. S. Proposal and Achievement of Novel Structure InN/GaN Multiple Quantum Wells Consisting of 1 ML and Fractional Monolayer InN Wells Inserted in GaN Matrix. *Appl. Phys. Lett.* **2007**, *90*, 073101.
43. Yoshikawa, A.; Che, S. B.; Yamaguchi, W.; Saito, H.; Wang, X. Q.; Ishitani, Y.; Hwang, E. S. Effect of Degree of Localization and Confinement Dimensionality of Excitons on Their Recombination Process in $CdSe/ZnSe/ZnS_xSe_{1-x}$ Single Quantum Well Structures. *Phys. Rev. B* **2000**, *61*, 10303–10313.
44. Chaisakul, P.; Marris-Morini, D.; Rouifed, M. S.; Frigerio, J.; Isella, G.; Chrastina, D.; Coudevylle, J.-R.; Roux, X. L.; Edmond, S.; Bouville, D.; *et al.* Strong Quantum-Confined Stark Effect from Light Hole Related Direct-Gap Transitions in Ge Quantum Wells. *Appl. Phys. Lett.* **2013**, *102*, 191107.
45. Cherevkov, S. A.; Fedorov, A. V.; Artemyev, M. V.; Prudnikau, A. V.; Baranov, A. V. Anisotropy of Electron−Phonon Interaction in Nanoscale CdSe Platelets as Seen *via* Off-Resonant and Resonant Raman Spectroscopy. *Phys. Rev. B* **2013**, *88*, 041303.
46. Kuo, Y. H.; Lee, Y. K.; Ge, Y. S.; Ren, S.; Roth, J. E.; Kamins, T. I.; Miller, D. A. B.; Harris, J. S. Strong Quantum-Confined Stark Effect in Germanium Quantum-Well Structures on Silicon. *Nature* **2005**, *437*, 1334–1336.
47. Miller, D. A. B.; Chemla, D. S.; Damen, T. C.; Gossard, A. C.; Wiegmann, W.; Wood, T. H.; Burrus, C. A. Electric Field Dependence of Optical Absorption near the Band Gap of Quantum-Well Structures. *Phys. Rev. B* **1985**, *32*, 1043–1060.
48. Kunneman, L. T.; Tessier, M. D.; Heuclin, H.; Dubertret, B.; Aulin, Y. V.; Grozema, F. C.; Schins, J. M.; Siebbeles, L. D. A. Bimolecular Auger Recombination of Electron−Hole Pairs in Two-Dimensional CdSe and CdSe/CdZnS Core/Shell Nanoplatelets. *J. Phys. Chem. Lett.* **2013**, *4*, 3574–3578.
49. Pedersen, T. G.; Lynge, T. B. Free-Carrier and Exciton Franz−Keldysh Theory for One-Dimensional Semiconductors. *Phys. Rev. B* **2002**, *65*, 085201.
50. Achtstein, A. W.; Hennig, J.; Prudnikau, A.; Artemyev, M. V.; Woggon, U. Linear and Two-Photon Absorption in Zero- and One-Dimensional CdS Nanocrystals: Influence of Size and Shape. *J. Phys. Chem. C* **2013**, *117*, 25756–25760.
51. Stokes, K. L.; Persans, P. D. Excited States and Size-Dependent Electro-optical Properties of CdS_xSe_{1-x} Quantum Dots. *Phys. Rev. B* **1996**, *54*, 1892–1901.
52. Sun, M.; Yang, X. Phosphine-Free Synthesis of High-Quality CdSe Nanocrystals in Noncoordination Solvents: "Activating Agent" and "Nucleating Agent" Controlled Nucleation and Growth. *J. Phys. Chem. C* **2009**, *113*, 8701–8709.
53. Prudnikau, A.; Artemyev, M.; Molinari, M.; Troyon, M.; Sukhanova, A.; Nabiev, I.; Baranov, A. V.; Cherevkov, S. A.; Fedorov, A. V. Chemical Substitution of Cd Ions by Hg in CdSe Nanorods and Nanodots: Spectroscopic and Structural Examination. *Mater. Sci. Eng., B* **2012**, *177*, 744–749.